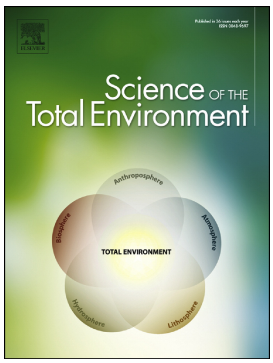


# Increased association between climate change and vegetation index variation promotes the coupling of dominant factors and vegetation growth

Wei Zhao, Xiubo Yu, Cuicui Jiao, Chengdong Xu, Yu Liu, Genan Wu

PII: S0048-9697(20)38200-0

DOI: https://doi.org/10.1016/j.scitotenv.2020.144669

Reference: STOTEN 144669

To appear in: *Science of the Total Environment*

Received date: 19 September 2020

Revised date: 15 December 2020

Accepted date: 15 December 2020

Please cite this article as: W. Zhao, X. Yu, C. Jiao, et al., Increased association between climate change and vegetation index variation promotes the coupling of dominant factors and vegetation growth, *Science of the Total Environment* (2020), https://doi.org/10.1016/j.scitotenv.2020.144669

# Increased association between climate change and vegetation index variation promotes the coupling of dominant factors and vegetation growth

Wei Zhao[1], Xiubo Yu[1,2,*], Cuicui Jiao[3], Chengdong Xu[1,2], Yu Liu[1,2], Genan Wu[1,2,4]

[1]Synthesis Research Center of Chinese Ecosystem Research Network, Key Laboratory of Ecosystem Network Observation and Modeling, Institute of Geographic Sciences and Natural Resources Research, Chinese Academy of Sciences, Beijing 100101, China

[2]College of Resources and Environment, University of Chinese Academy of Sciences, Beijing 100190, China

[3]College of Economics, Sichuan University of Science & Engineering, Yibin 644000, China

[4]Lawrence Berkeley National Laboratory, Berkeley, CA, USA

*Corresponding author: Xiubo Yu, E-mail: yuxb@igsnrr.ac.cn

# Increased association between climate change and vegetation index variation promotes the coupling of dominant factors and vegetation growth


## Abstract

Vegetation productivity dynamics are closely related to climate change, and water availability determines vegetation growth in water-limited ecosystems. Nevertheless, how changes in the interactions between climatic factors and vegetation activity variation regulate the relationship between their trends remains unclear. The Normalized Difference Vegetation Index (NDVI) is an effective proxy of vegetation growth. First, we investigated the NDVI trends, and the results revealed a vegetation activity with weaker greening and greater spatial heterogeneity after an obvious land-cover breakpoint in 1999 compared with that before 1999 in northwest China. Notably, the Loess Plateau greatly led the greenness trends, but the Tibet Plateau showed mean browning after 1999, which implied that the coupling of climate change and vegetation trends varied with spatio-temporal changes. Subsequently, using the Geographical Detector Method (GDM), we quantified and compared the association between climate change and the interannual variability of NDVI in the two stages. Vegetation productivity variation is more closely related to changes in climatic factors after 1999 compared with that before 1999. Precipitation (PPT) and vapor pressure deficit (VPD) are the primary constraints to vegetation growth in both stages. Patterns in NDVI trend increases are consistent with those of increased PPT and decreased VPD and vice versa after 1999. However, the same patterns were not observed before 1999 because of the weak association between climate change and NDVI variation.

This implicated a great significance of the association between climate change and changes in vegetation activity for the prediction of potential carbon sequestration due to the shift of dominant factors and their trends under future climate change.

**Keywords:**

NDVI interannual variability; land-surface cover breakpoint; quantified association; explanatory power; dominant climatic factors; northwest China

## 1 Introduction

Climate change, including interannual variation and trends (Ryo et al., 2019), is regarded as one of the drivers of vegetation activity (Schimel et al., 2000; Zhou et al., 2001; Nemani et al., 2003) and is affected by land surface cover changes and vice versa. Generally, increasing precipitation would enhance vegetation growth in water-limited ecosystems; in turn, surface greening would create biophysical feedback to the climate that would increase evapotranspiration, and subsequently, surface cooling and precipitation (Davin et al., 2010; Yu et al., 2020). Trends in the dominant climatic factors are expected to play critical roles in the spatial and temporal patterns of vegetation growth, but how the interplay between climate change and changes in vegetation activities regulate the relationship between climatic factors and vegetation growth trends remains unclear.

Greening (Piao et al., 2015; Zhu et al., 2016; Chen et al., 2019) and deforestation (Davin et al., 2010; Strassburg et al., 2012; Seymour et al., 2019) has occurred globally

over the past several decades. The dominant climatic driver of vegetation dynamics and its feedback to the climate were investigated. Rapid warming has resulted in a 16.4% decline in the vegetation land area limited by temperature in cold and high-latitude ecosystems (Keenan & Riley, 2018). The precipitation threshold for water limitation of vegetation cover significantly declined from 1982 to 2010 in Australia as the vegetation subsequently adapted (Ukkola et al., 2015). Surface warming and cooling effects were observed due to deforestation and surface greening, respectively (Davin et al., 2010; Yu et al., 2020). The biogeophysical effects of re-afforestation throughout Europe include uncertainty over the diverging responses in summer temperature changes (Davin et al., 2020). Global warming would exceed the optimal temperature for vegetation growth, resulting in limited safe operating space for these ecosystems (Huang et al., 2019; Xu et al., 2013). Therefore, dominant climatic factors varied spatially and temporally, leading to potential differences in vegetation activity with climate change and spatial variation. Changes in the association between climate change and vegetation activity variation could change the dominant climatic factors, leading to a variation in plant growth.

Vegetation growth trends are spatially heterogeneous and closely related to climatic factors. The spatial extent of vegetation productivity in a water-limited grassland is consistent with annual precipitation distribution (Piao et al., 2006). From 1981–2007, average greening was observed across the global semi-arid areas (0.015 NDVI (Normalized Difference Vegetation Index)), both in areas where precipitation was the dominant factor of plant production (0.019 NDVI) and air temperature was the primary growth constraint (0.013 NDVI). However, their explanations differ widely,

and the local and regional trends reveal considerable variation in the direction and magnitude of change (Fensholt et al., 2012). It is suggested that surface vegetation growth trends are complicated by the dominant factors, and greenness could occur in regions where either precipitation or temperature limit vegetation activities. The interaction between vegetation dynamics and climate change leads to potential adaptation and feedback in the vegetation–climate system. Exploring the changes in the degree of the association between climatic factors and vegetation activity and how it regulates their trends in a region where an evident surface greenness shift has occurred is important for predicting the response and adaptation of the carbon cycle to climate change. Northwest China provides a potential platform for identifying the spatial and temporal variation in vegetation growth trends and the interaction between vegetation dynamics and climate change, as considerable breakpoints in vegetation growth were observed in most regions in 1999 (Liu et al., 2019).

The response and relationship between climate change and vegetation activity are uncertain but vary with spatio-temporal changes in disturbance, such as human activities and terrain. Warming has increased the carbon cycles of the Tibetan Plateau but not of the Inner Mongolia grasslands; this is because vegetation growth is constrained by temperature in the Tibetan Plateau and water in the Inner Mongolia region (Liu et al., 2018). The NDVI increase rate was lower during 2000–2010 than during 1982–1999 (Piao, 2003; Peng et al., 2011). The largest greening and browning trends are found in southwest China and northeastern Inner Mongolia (Piao et al., 2015), respectively. A shift in dominant climatic factors to vegetation dynamics is a key

indicator for predicting future vegetation activity under climate change. Ecological restoration programs have enhanced surface vegetation greening (Piao et al., 2015), but whether vegetation planting increases carbon sequestration (Baldocchi & Penuelas, 2019) or causes high water consumption (Cao, 2008; Chen et al., 2015; Wang et al., 2019) in the long run is debated. The association between climate change and vegetation activities is highly related to global ecosystem sustainability. However, the association role between climate change and changes in vegetation activity in the evolution of the climate–vegetation system remains poorly understood. In the present study, we compared two periods before and after 1999 stage I; 1982–1998 and stage II; 1999–2015. First, we investigated the divergent patterns in NDVI trends and their spatial distribution in four sub-regions. Second, we quantified the association between climate change and changes in vegetation activities. Lastly, we explored the trends' characteristics in both vegetation growth and dominant climatic factors in terms of changes in the degree of the association between climate change and changes in vegetation activity.

## 2 Materials and Methods

### 2.1 Study region

This study was conducted in northwest China (25°59′N–53°19′N, 73°26′E–125°59′E) and included four geographical subregions (Figure 1a): Inner Mongolia (IM), Loess Plateau (LP), Tibetan Plateau (TP), and Xinjiang (XJ); these corresponded to 21.91%, 6.97%, 53.99%, and 17.13% of the total area, respectively. Grasslands were

abundant in most of these regions, with temperate grasslands mainly distributed in IM, LP, and XJ, and alpine grasslands distributed in the TP (Zhao et al., 2019), which contained scattered, sparse forest and shrub. To mitigate the effects of desertification and dust storms, the Chinese government implemented large-scale ecological restoration projects in the study region; e.g., the Three-North Shelterbelt Project (TNSP) (Li et al., 2012), Grain for Green Project (GGP) (Feng et al., 2016), and Beijing-Tianjin Sand Source Control Project (BSSCP) (Wu et al., 2014). Most of the study region is typically characterized by arid and semi-arid climate, and TP has a typical cold and dry alpine climate. The mean annual temperature and mean annual precipitation range from −3 to 9 ℃ and 100 to 700 mm, respectively (Zhang et al., 2016).



**2.2 Meteorology dataset**

Gridded total precipitation (PPT) and average monthly value of air temperature (Ta), vapor pressure deficit (VPD), and solar radiation (SR) at each growing season (from May to September) during 1982–2015 at 10 km resolution were analyzed in this study. Data on daily Ta, PPT, and actual sunshine duration recorded by 756 nationwide stations were obtained from the China Meteorological Data Service Center (http://data.cma.cn/en). Site-level daily short radiation was calculated using the Ångström formula, which is the algorithm recommended by the Food and Agriculture Organization (http://www.fao.org/docrep/x0490e/x0490e07.htm#radiation). This relates short radiation to extraterrestrial radiation and the relative sunshine duration,

which is calculated using the actual sunshine duration to remove the impact of clouds. The site data of daily VPD was calculated by measuring Ta and relative humidity (RH) (Howell & Dusek, 1995):

$$VPD = 0.611 \times e^{\frac{17.27 \times T_a}{T_a + 237.3}} \times (1 - \frac{RH}{100})$$

Furthermore, data obtained from the sites were interpolated to 10 km and 15-day resolutions throughout the nation using the ANUSPLIN software package (Hutchinson & Xu, 2013), which provides an interpolation of noisy multivariate data using thin-plate smoothing splines from observation data acquired from meteorological stations. ANUSPLIN is widely used for the interpolation of climatic variables (Ukkola et al., 2015). The quality of the interpolated meteorological dataset has been fully evaluated and has reliable accuracy (Yu et al., 2004).

**2.3 NDVI dataset**

NDVI is associated with surface cover change and is generally used to evaluate the temporal and spatial patterns of vegetation activity (Huang et al., 2019; Piao et al., 2015). The GIMMS (Global Inventory Modelling and Mapping Studies) NDVI3g dataset is now available covering 1982–2015 with an 8 km spatial resolution and a bimonthly temporal resolution (Pinzon & Tucker, 2014); this has proved efficacious in representing plant growth owing to their long time-series record (Fensholt & Proud, 2012; Tian et al., 2015). NDVI is a good indicator of surface vegetation cover, and increasing and decreasing NDVI is referred to as “greening” and “browning,” respectively (Alcaraz-Segura et al., 2010). Grids with a mean NDVI >0.1 in any

growing season were selected as available units, and all farmland grids were removed according to the land use map (http://www.resdc.cn/) from 1982 to 2015. A significance level of $p < 0.05$ was used. We calculated the mean NDVI of the annual growing season (May–September) using the average value of monthly NDVI resampled with the nearest-neighbor method using ArcGIS 10.2 software at the same spatial resolution (10 km) as the meteorological data.

### 2.4 Trends detection

The non-parametric Mann-Kendal (M-K) (Kendall, 1975; Mann, 1945) and Pettitt tests were applied to examine the trends in NDVI and climatic factors at the pixel scale in the study region for stages I and II. The average NDVI trend was the mean value of NDVI trends in all grids across the study region.

The M-K test measures the degree to which a trend is generally increasing or decreasing and is not subject to a particular distribution nor outliers dataset and has been widely used in climatology and ecology (Fansholt et al., 2012; Ely Yacoub et al., 2019; Araminiene et al., 2019; Wingate et al., 2019; de Oliveira Serrão et al., 2020). Furthermore, the Shapiro–Wilk test was performed for the NDVI time series to confirm normal distribution in the dataset. The specific statistical value (S) and standardized test statistics (ZMK) were calculated as follows:

$$S = \sum_{i=1}^{n-1} \sum_{j=i+1}^{n} \mathrm{sgn}(X_j - X_i)$$

$$\mathrm{sgn}(X_j - X_k) = \begin{bmatrix} +1 (X_j - X_k) > 0 \\ 0 (X_j - X_k) = 0 \\ -1 (X_j - X_k) < 0 \end{bmatrix}$$

amongst,

$$Z_{MK} = \begin{cases} \dfrac{S-1}{\sqrt{Var(S)}} & if\ S > 0 \\ 0 & if\ S = 0 \\ \dfrac{S+1}{\sqrt{Var(S)}} & if\ S < 0 \end{cases}$$

where ZMK >0 shows an increasing trend with time and vice versa, and if |ZMK| is >1.96 ($p < 0.05$), then the null hypothesis is rejected, and a significant trend is observed and vice versa.

**2.5 Association between climatic factors and vegetation dynamics**

The Geographical Detection Method (GDM) was used to quantify the association between each climatic factor and interannual variation (IAV) of vegetation dynamics in a grid in the study region. The method is a type of variance analysis that can measure spatial heterogeneity and detect potential factors (Wang et al., 2010). The GDM does not require a linear hypothesis to identify the explanatory power behind stratified heterogeneity and has been widely applied in studies of ecological processes and geographic applications (Zhao et al., 2019; Luo et al., 2019; Ding et al., 2019; Zhao et al., 2020). Using the K-means classification algorithm, we discretized the numerical variables into categorical groups as the stratum of NDVI and climatic factors in GDM. The explanatory power for each climatic variable ($x$) on the IAV of NDVI was quantified by the indicator ($q$):

$$q_x = 1 - \frac{\sum_{i=1}^{m} N_i \sigma_i^2}{N\sigma^2} = 1 - \frac{SSW}{SST}$$

where $q_x$ ($\in [0,1]$) is the explanatory power of the climatic factor $x$; $i$ = 1,…; $m$ is the stratum (category) of NDVI for the climatic factor $x$; $N_i$ and $N$ are the total sample numbers of the $i$ stratum and overall period (1982–1998 or 1999–2015), respectively; $\sigma_i^2$ and $\sigma^2$ are the variances of NDVI in the $i$ stratum and overall period, respectively; SSW and SST are the within sum of squares in the $i$ stratum and total sum of squares in the overall period, respectively.

**2.6 Data analysis**

Using the M-K method and GDM, we detected the vegetation trends and identified the dominant factors in both stages. There were four reasons for choosing 1999 as the breakpoint. First, the three ecological restoration programs (GGP, NFCP, and BSSCP) were implemented around 1999 following the TNSP (Feng et al., 2016). Second, a pronounced surface greening breakpoint was detected in 1999 in most areas where ecological restoration programs had been implemented (Niu et al., 2019). Third, after the late 1990s, there was a sharp global increase in VPD (Li et al., 2018), an important driver of atmospheric water availability for plant growth (Rawson et al., 1977). Lastly, the two periods before and after 1999 were both 17 years, ensuring the same sample sizes and convincing contrast analysis.

## 3 Results

### 3.1 Divergent Spatial distribution of NDVI trends before and after 1999

The mean value of NDVI trends across the whole study region was 1.02 ± 0.01‰ $yr^{-1}$ in stage Ⅰ but was lower (0.64 ± 0.01‰ $yr^{-1}$) in stage Ⅱ (Figure 1b). In contrast, the variation coefficient for all pixel NDVI trends was 4.19 in stage II and 1.34 in stage I. Average NDVI trends increased by 1.06 ± 0.01‰ $yr^{-1}$ and 1.32 ± 0.02‰ $yr^{-1}$ (IM); 1.48 ± 0.03‰ $yr^{-1}$ and 5.62 ± 0.07‰ $yr^{-1}$ (LP); and 1.09 ± 0.02‰ $yr^{-1}$ and 0.36 ± 0.03‰ $yr^{-1}$ (XJ) in stages Ⅰ and Ⅱ, respectively. Meanwhile, the average NDVI trends on TP were positive (0.96 ± 0.01‰ $yr^{-1}$) in stage Ⅰ and negative (−0.19 ± 0.01‰ $yr^{-1}$) in stage Ⅱ.

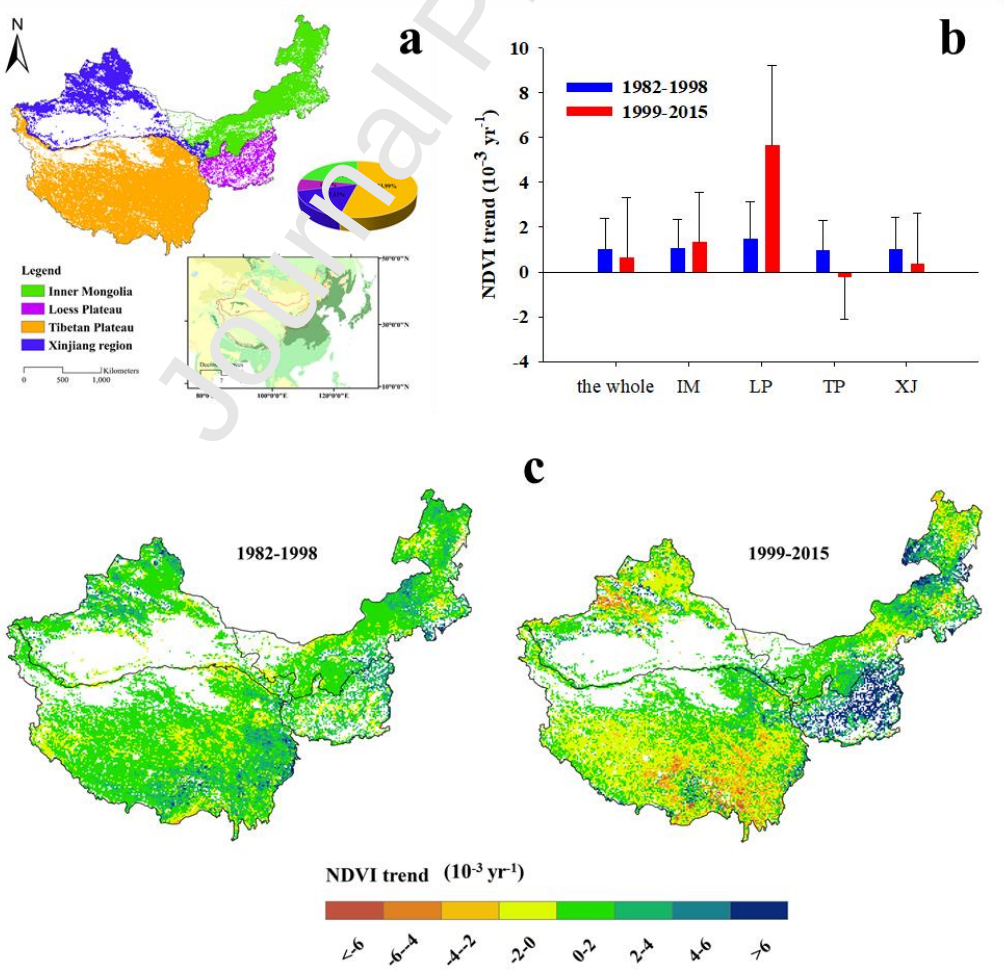

**Figure 1. (a) The location of the study region and its subregions, (b) the average NDVI trends, (c) and its spatial distribution before and after 1999. (a)** Pie chart shows the ratio of the area of four subregions: Inner Mongolia (IM), Loess Plateau (LP), Tibetan Plateau (TP), and Xinjiang areas (XJ). **(b)** Bars denote the average NDVI trends in stage I (blue) and stage II (red) in the whole region and its subregions. The error bars represent standard deviations.

The increase in positive NDVI trends was similar to the decrease in negative NDVI trends for the whole region in stage II compared with that in stage I, but in IM and LP, the increase in positive NDVI was higher than the decrease in negative NDVI (Figure 2). NDVI trends in the whole region increased from $1.34 \pm 1.26‰\ yr^{-1}$ to $2.09 \pm 2.42‰\ yr^{-1}$ and decreased from $-0.54 \pm 0.65‰\ yr^{-1}$ to $-1.38 \pm 1.38‰\ yr^{-1}$. For positive NDVI trends, the average value increased from $1.33 \pm 1.19‰\ yr^{-1}$ (stage I) to $2.14 \pm 1.90‰\ yr^{-1}$ (stage Ⅱ) in IM and from $1.92 \pm 1.35‰\ yr^{-1}$ (stage I) to $5.94 \pm 3.32‰\ yr^{-1}$ (stage Ⅱ) in LP. In contrast, for negative NDVI trends, the average value decreased from $-0.45 \pm 0.65‰\ yr^{-1}$ (stage I) to $-1.2 \pm 1.07‰\ yr^{-1}$ (stage Ⅱ) in IM and from $-0.58 \pm 0.64‰\ yr^{-1}$ (stage I) to $-1.42 \pm 1.41‰\ yr^{-1}$ (stage Ⅱ) in LP. Additionally, the magnitude of the increase in positive NDVI trends was less than that of the decrease in negative NDVI trends for TP and XJ in stage II compared with those in stage I.

Areas of positive NDVI trends (greening) were reduced in stage Ⅱ compared with those of stage Ⅰ, except for in LP. The frequency of the NDVI trend was flatter in stage Ⅱ than that in stage Ⅰ for each region (Figure 2). The area percentage of greening decreased from 82.8% to 58.0% in the whole region in stage II than in stage I. The area

percentage exhibited the highest reduction in greening from 82.6% to 46.2% in TP, followed by 82.8% to 59.2% in XJ, and the smallest reduction was from 85.1% to 75.5% in IM in stage II compared with that in stage I. However, increased greening was observed in LP (84.0% and 96.0% of the area before and after 1999, respectively). In stage II, the TP region dominated the decreased greening area of the whole region due to the large reduction in greening area.

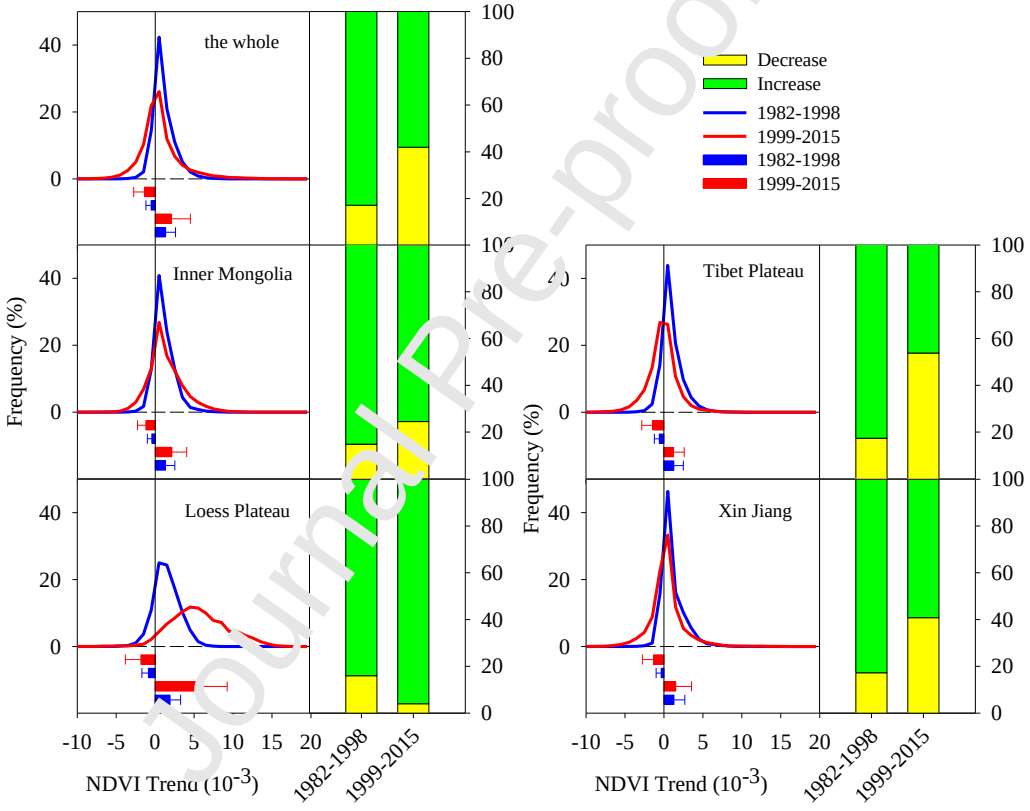


**Figure 2. The frequency, area percentage, and mean value of NDVI trends before and after 1999.** Lines denote the frequency of NDVI trends in stage I (blue) and stage II (red). Horizontal bars denote the average magnitude of negative and positive NDVI trends in stage I (blue) and stage II (red), respectively. Histograms denote the area percentages of NDVI increase (green) and decrease (yellow). The error bars represent standard deviations.

### 3.2 Association between climate change and the IAV of NDVI

In the study area, the area percentages of each dominant factor in stages Ⅰ and Ⅱ were similar, but the total explanatory power of the four climatic factors to the IAV of NDVI (sum of the mean explanatory power of PPT, SR, Ta, and VPD in the grid) in stage II (71.3%) was higher than that in stage I (63.2%). In the whole study region, the average explanatory power of PPT was 17.0% and 19.5%, that of SR was 13.9% and 14.6, and that of Ta was 14.3% and 17.0%, in stages I and II, respectively; these values were higher in stage II compared to stage I. Climatic variability regulated vegetation dynamics more strongly in stage Ⅱ than stage Ⅰ.

For each subregion, the PPT area as the dominant factor, accounted for larger percentages in stage Ⅱ than stage Ⅰ with 41.3% and 36.6% in IM, 33.8% and 24.7% in LP, 21.7% and 20.6% in TP, respectively; however, the opposite was observed in XJ with 34.6% and 36.9% in stages II and I, respectively (Figure 3). Meanwhile, the area percentages of SP as the dominant factor were lower in stage II than those in stage I with 9.1% and 18.0% in IM, 15.5% and 19.3% in LP, 14.0% and 21.7% in XJ, respectively; however, the opposite was observed in TP with 26.5% and 21.5% in stages II and I, respectively. Furthermore, Ta as the dominant factor accounted for relatively similar area percentages in stages Ⅱ and Ⅰ, which were 15.4% and 13.6% in IM, 24.5% and 25.9% in LP, 29.4% and 25.4% in TP, and 18.8% and 20.2% in XJ, respectively. It is noted that VPD as the dominant climatic factor accounted for equal or more area percentage than PPT, which was 30.0% and 36.0% in IM, 22.6% and 31.2%

in XJ, 31.4% and 24.8% in LP, and 28.5% and 26.4% in TP in stages I and Ⅱ, respectively (Figure 3).

Meanwhile, the average explanatory power of PPT in stage II was higher than that in stage I, which was 30.6% and 24.8% in IM, 20.8% and 16.1% in LP, and 14.6% and 12.7% in TP, respectively; however, the opposite was observed in XJ with 20.3% and 21.2% in stages II and I, respectively (Figure 3). The average explanatory power pattern of SR was similar in the two stages and four subregions and was similar to their area percentage distribution. Additionally, Ta variability in stage Ⅱ contributed more to the IAV of NDVI than that of stage Ⅰ: 20.3% and 12.7% in IM, 18.1% and 14.2% in LP, 16.0% and 14.8% in TP, and 15.8% and 14.3% in XJ, respectively. Interestingly, the IAV of NDVI for all regions was explained by VPD more substantially in stage Ⅱ than in stage I, the explanatory power was 29.2% and 23.5% in IM, 19.1% and 17.9% in LP, 16.4% and 15.7% in TP, and 20.4% and 17.7% in XJ, respectively.

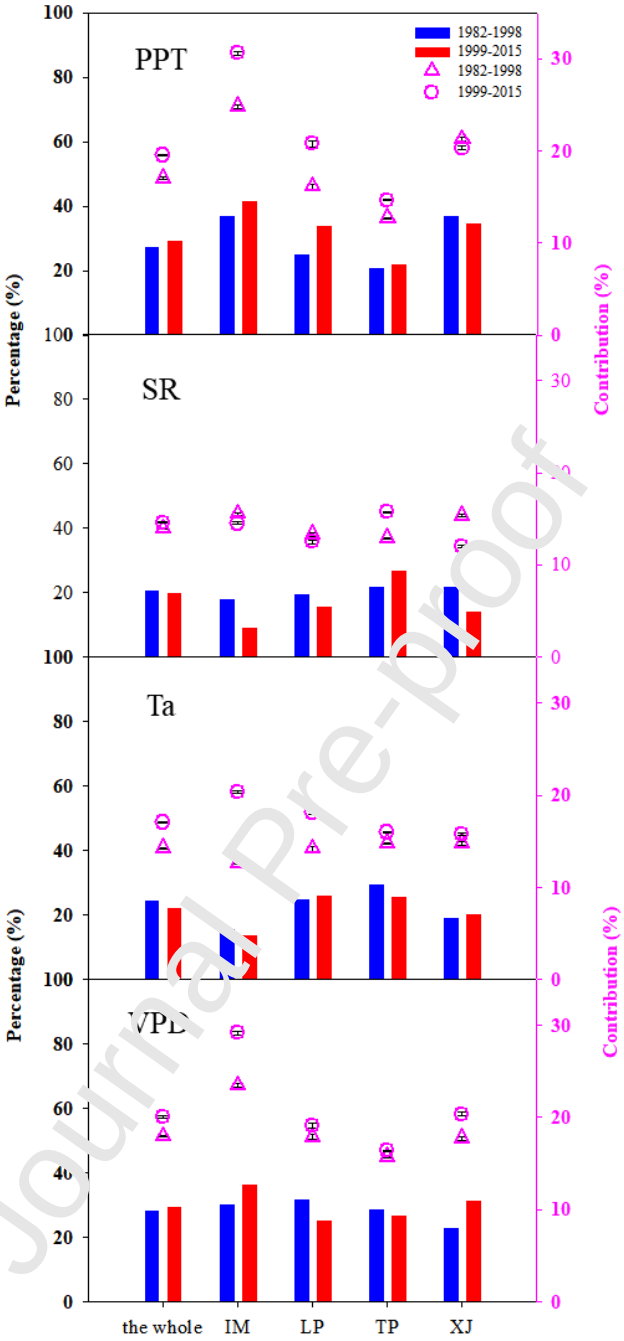


**Figure 3. The area percentage of dominant climatic factors and the mean value of explanatory powers between four climatic factors and the IAV of NDVI in each region.**

Bars denote the area percentage of PPT, SR, Ta, and VPD as the dominant climatic factors in stage I (blue) and stage II (red). Circles and triangles denote the average explanatory powers of four climatic factors (PPT, SR, Ta, and VPD) in stages I and II, respectively, in the whole study

region and its four subregions (IM: Inner Mongolia; LP: Loess Plateau; TP: Tibetan Plateau; XJ: Xinjiang).

### 3.3 NDVI trends coupled with dominant climatic factors

Figures 4a and 4b show that NDVI trends intensified with increasing NDVI, and the pattern of the NDVI distribution curve was much flatter in stage Ⅱ than in stage I. When the NDVI trend was 0–3‰ $yr^{-1}$, the average NDVI was from 0.20 to 0.48 in stage I and 0.21 to 0.39 in stage Ⅱ. In contrast, when the NDVI trend was −3–0‰ $yr^{-1}$, the average NDVI was from 0.50 to 0.17 in stage I and 0.48 to 0.22 in stage II. It was noted that a higher average NDVI was observed in stage I than in stage II when much greening occurred (NDVI trend >1‰ $yr^{-1}$). Moreover, the area of greening with an average of 0.2–0.4 NDVI value was greater in stage II (79.4%) than in stage I (65.8%).

Figures 4c and 4d indicate that the association between climatic factors and vegetation dynamics increased with the intensifying NDVI trends in stage II. Nevertheless, the same pattern was not observed in stage I. However, what is relevant is that the explanatory power between PPT and VPD and the IAV of NDVI was mostly higher than that of each factor in stage I. Furthermore, with the NDVI trend of −3–3‰ $yr^{-1}$, the average PPT and VPD trends were less marked and narrowed in scope in stage I than in stage II. They were −0.69 to 1.47 mm $yr^{-1}$ and −0.007 to 0.019 hpa $yr^{-1}$ in stage I; and −1.07 to 3.13 mm $yr^{-1}$ and −0.018 to 0.037 hpa $yr^{-1}$ in stage II, respectively (Figure 4e, 4f). Specifically, the PPT trend increased, and VPD decreased; this was strengthened by coupling with the increasing NDVI trend in stage II. However, this

pattern was not observed in stage I, in which both the PPT and VPD trends only slightly fluctuated. No obvious differences were observed for the average explanatory power of Ta and SR between stages I and II.

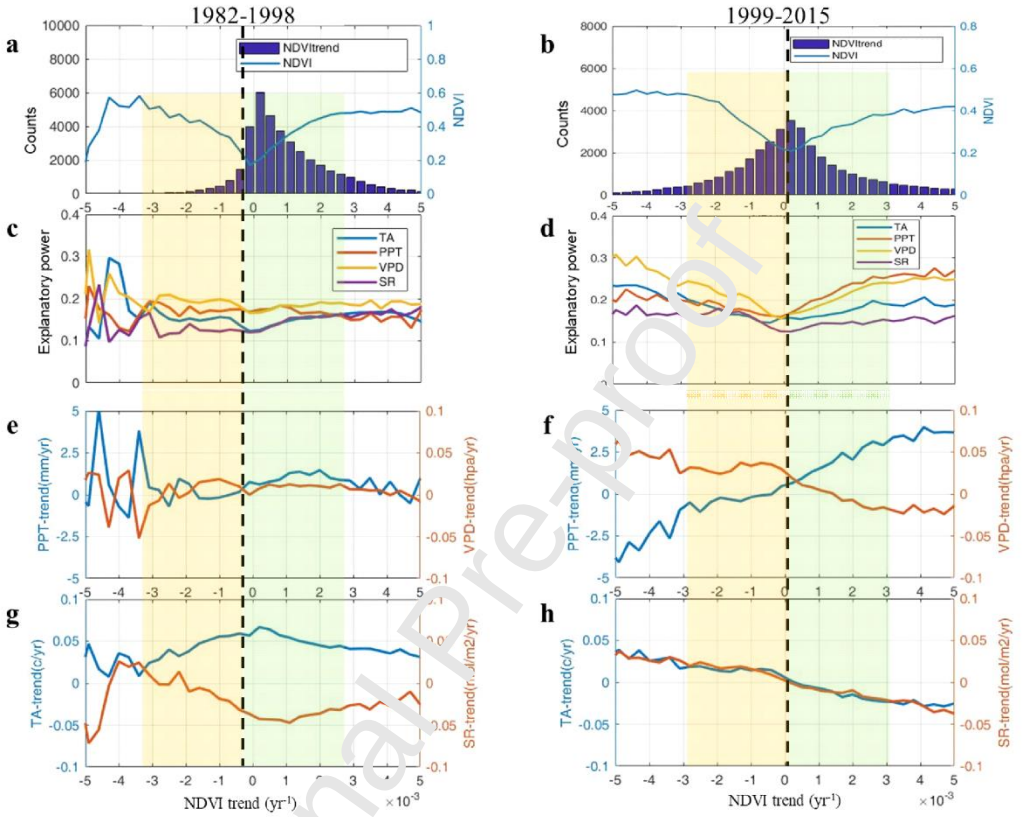


**Figure 4. The pattern of NDVI, the average explanatory power between climate change and the IAV of NDVI, and trends of the climatic factors following NDVI trends.** (**a**) and (**b**) shows the frequency of NDVI trends (bars) and the average NDVI following the corresponding NDVI trend group in stages I and II, respectively. (**c**) and (**d**) shows the average explanatory powers of four climatic factors (blue line: Ta; red line: PPT; orange line: VPD; purple line: SR) following the corresponding NDVI trend group. (**e**) and (**f**) shows the average trends of PPT (blue line) and VPD (orange line). (**g**) and (**h**) shows the average trends of Ta (blue line) and SR (orange line) following the corresponding NDVI trend group.

## 4 Discussions

### 4.1 Divergent spatial distribution of NDVI trends

We investigated NDVI trends and found a prevalent greening during 1982–2015 and a divergent spatial distribution of NDVI trends before and after 1999. Since 1999, the ecological restoration has had a positive effect on surface greening (Niu et al., 2019; Wu et al., 2014) in northwest China, which confirmed our results of greening in this region. However, the average increasing rate of NDVI was lower after 1999 than before 1999, as the area of greening (positive NDVI trends) reduced and the magnitude weakened across the whole region in stage II. For subregions, the LP largely led the increased greening in both area and amplitude of positive NDVI trends after 1999; this is consistent with the considerable improvement in vegetation dynamics following revegetation programs since 1999 (Feng et al., 2016; Li et al., 2017). Notably, in stage II, the vegetation was browning in TP, which was explained by the occurrence of severe droughts (Wu et al., 2014). Nonlinear changes in surface greenness were detected in eastern Inner Mongolia, human activities drove the increasing phase, and droughts induced the decreasing phase (Ding et al., 2020).

These results highlight that greening occurred consistently in northwestern China over the past decades in spatially and temporally heterogeneous patterns, especially in LP with significant greening and in TP with slight browning from 1999 to 2015, relative to that from 1982 to 1998. This result suggested that although China has been

leading global greening in the past decades (Chen et al., 2019), more attention should be paid to the spatial heterogeneity of NDVI trends, which would lead to land degradation and ecosystem shifts, especially in regions that are fragile to global change (Berdugo et al., 2020). Determining how to assess the spatial variability and its ecological mechanism with long-term field observations is urgently required.

**4.2 Increased explanatory power between climate change and the IAV of NDVI**

In northwest China, the association between climatic variation and vegetation dynamics was enhanced in 1999–2015 compared with 1982–1998. The average explanatory powers of PPT and Ta and the IAV of NDVI were largely increased after 1999 compared with those before 1999, especially in IM and LP. This is because enhanced vegetation restoration and regrowth reduced surface runoff and soil erosion (Deng et al., 2012; Farley et al., 2005; Wang et al., 2015; Zhang et al., 2016) and consequently improved water use efficiency (Ukkola et al., 2015; Zhang et al., 2016; Zheng et al., 2019). This led to a higher explanatory power for precipitation change and the IAV of NDVI at the regional scale than the previous sparse vegetation. Furthermore, increased drought events resulted in the increased atmospheric aridity in IM (Piao et al., 2015). Land–atmosphere feedbacks could exacerbate soil drought and atmospheric aridity (VPD increasing) and, consequently, severe constrain terrestrial carbon uptake in stage II (Zhou et al., 2019). Additionally, increased precipitation not only enhanced ecosystem carbon fluxes but also mitigated the negative effects of climate warming on ecosystem carbon fluxes. Vegetation regrowth could produce a negative feedback effect on warming, which would probably be attributed to increased

evapotranspiration resulting from increased NDVI (Bonan, 2008; Zhao et al., 2017). These results suggested that the potential advantageous revegetation in response to climate change enhanced the total explanatory power of each other.

Greater coupling of vegetation growth with dominant factor variation was observed after 1999 compared with before 1999 in northwest China. The favorable water conditions enhanced sustainability and environmental benefits, and climate change played an additive role in strengthening vegetation growth trends. In the semi-arid region, greening was considered a response to increasing precipitation, which was the dominant factor of the IAV of NDVI (Peng et al., 2013). Browning was observed where VPD was the dominant factor since intensified atmospheric aridity had constrained vegetation growth by affecting plant photosynthesis over the past decades (Yuan et al., 2019). In the present study, the results after 1999 indicated that the distribution pattern of NDVI trends was consistent with that of changes in dominant climatic factors, and the positive NDVI trends corresponded with increasing PPT and decreasing VPD trends (Figure 4). However, the same pattern was not observed before 1999, owing to the weak explanatory power of climate change and the IAV of NDVI. Although PPT and VPD are the dominant factors of vegetation activities either before or after 1999, the increased association between climate change and the IAV of NDVI enhanced the coupling of climate change and vegetation growth after 1999 compared with that before 1999. Ecological projects have changed the surface energy balance and created an external disturbance in land surface–atmospheric feedbacks, and improved the association between climate change and vegetation activities and their dependence

on one another. Additionally, $CO_2$ fertilization positively affected vegetation growth, but interannual variation in $CO_2$ concentration was relatively stable, and also hot drought reduced the effect of $CO_2$ elevation on tree water use efficiency and carbon metabolism (Birami et al., 2020).

Climate–vegetation interactions were regarded as the critical core of the terrestrial ecosystem carbon cycle, especially in water-limited ecosystems that are sensitive to climate change (Seddon et al. 2016), such as drylands that dominate the interannual variability in global carbon sinks (Poulter et al., 2014; Ahlström et al. 2015). Global dry areas showed high NDVI variability, and an increase in the IAV of vegetation greenness was observed over time which was primarily driven by climate change without considering human disturbance (Chen et al., 2019). In turn, the biophysical effects of greening on climate change were widely reported as either cooling or warming the surface in different climatic zones (Forzieri et al., 2017; Chen et al., 2020). The future trajectories of the vegetation–atmosphere system are likely to coevolve even more closely than that at present (Forzieri et al., 2017), an assertion that was supported by the present study. Our results indicated that the increased strength of the association between climate change and vegetation activity variation could improve surface greening under favorable dominant climate trends and vice versa. Uncertainties remain regarding the sustainable adaptation of vegetation growth to climate change. First, there is uncertainty over regional water storage assessments. This is closely related to the regrowth of planted vegetation and is greatly affected by climate change characteristics (Feng et al., 2016), including surplus precipitation and

an increase in drought. Second, there is a more effective way to understand the mechanism underlying the climate–vegetation feedbacks, including the influences of seasonal rainfalls, drought events, and even frost, which are all important for vegetation growth in arid and semi-arid regions. Lastly, vegetation dynamics represent a comprehensive response to climate change, and the interaction between climatic factors and vegetation dynamics should be paid more attention to in the future. Long-term monitoring across ecosystems and an integrated process model, including vegetation traits and their response to climate change, are key to improving our predictions of how ecosystems respond to global change.

## 5 Conclusions

Average greening was observed in northwest China in both stages (1982–1998 and 1999–2015). However, divergent spatial distribution of NDVI trends was evident with much more heterogeneity in the whole region after 1999 than before 1999. After 1999, LP played an important role in leading the greenness trends, both in the area of greening and the amplitude of positive NDVI trends. Conversely, average browning was observed in TP. This suggested that the coupling of the climate–vegetation system varied with tempo-spatial changes. The association of climate variation with the IAV of NDVI was quantified and strengthened in stage II (1999–2015) than in stage I (1982–1998). Although water availability was the dominant factor for vegetation growth in both stages, the increased association between climate change

and changes in vegetation activity enhanced the coupling of dominant factors with vegetation growth trends after 1999. Dominant factors affected the positive NDVI trend pattern due to increasing PPT and decreasing VPD after 1999 but not before 1999, owing to their weak explanatory power. Our results imply the significance of the degree of association between climate change and vegetation dynamics for predicting ecosystem carbon storage variation.



## Acknowledgments

This work was supported by the International Partnership Program of the Chinese Academy of Sciences (Grant No. 121311KYSB20170004), the National Postdoctoral Fund (2020M670439). The authors declare no conflicts of interest. The NDVI data were obtained from https://ecocast.arc.nasa.gov/data/pub/gimms/3g.v1/. The climate data were obtained from http://data.cma.cn/en.

## References

Ahlström A, Raupach MR, Schurgers G, Smith B, Arneth A, Jung M, et al. The dominant role of semi-arid ecosystems in the trend and variability of the land $CO_2$ sink. Science 2015; 348: 895-899.

Alcaraz-Segura D, Chuvieco E, Epstein HE, Kasischke ES, Trishchenko A. Debating the greening vs. browning of the North American boreal forest: differences between satellite datasets. Global Change Biology 2010; 16: 760-770.

Araminiene V, Sicard P, Anav A, Agathokleous E, Stakenas V, De Marco A, et al. Trends and inter-relationships of ground-level ozone metrics and forest health in Lithuania. Sci Total Environ 2019; 658: 1265-1277.

Baldocchi D, Penuelas J. The physics and ecology of mining carbon dioxide from the atmosphere by ecosystems. Glob Chang Biol 2018; 25: 1191-1197.

Berdugo M, Delgado-Baquerizo M, Soliveres S, Hernandez-Clemente R, Zhao Y, Gaitan JJ, et al. Global ecosystem thresholds driven by aridity. Science 2020; 367: 787-790.

Birami B, Nagele T, Gattmann M, Preisler Y, Gast A, Arneth A, et al. Hot drought reduces the effects of elevated $CO_2$ on tree water-use efficiency and carbon metabolism. New Phytol 2020; 226: 1607-1621.

Bonan GB. Forests and climate change: forcings, feedbacks, and the climate benefits of forests. Science 2008; 320: 1444-9.

Cao S. Why large-scale afforestation efforts in China have failed to solve the desertification problem. Environ Sci Technol 2008; 42: 1826-31.

Chen C, He B, Yuan WP, Guo LL, Zhang YF. Increasing interannual variability of global vegetation greenness. Environmental Research Letters 2019a; 14.

Chen C, Li D, Li Y, Piao S, Wang X, Huang M, et al. Biophysical impacts of Earth greening largely controlled by aerodynamic resistance. Sci Adv 2020; 6.

Chen C, Park T, Wang X, Piao S, Xu B, Chaturvedi RK, et al. China and India lead in greening of the world through land-use management. Nat Sustain 2019b; 2: 122-129.

Chen YP, Wang KB, Lin YS, Shi WY, Song Y, He XH. Balancing green and grain trade. Nature Geoscience 2015; 8: 739-741.

Davin EL, de Noblet-Ducoudre N. Climatic Impact of Global-Scale Deforestation: Radiative versus Nonradiative Processes. Journal of Climate 2010; 23: 97-112.

Davin EL, Rechid D, Breil M, Cardoso RM, Coppola E, Hoffmann P, et al. Biogeophysical impacts of forestation in Europe: first results from the LUCAS (Land Use and Climate Across Scales) regional climate model intercomparison. Earth System Dynamics 2020; 11: 183-200.

de Oliveira Serrao EA, Silva MT, Ferreira TR, de Paulo Rodrigues da Silva V, de Salviano de Sousa F, de Lima AMM, et al. Land use change scenarios and their effects on hydropower energy in the Amazon. Sci Total Environ 2020; 744: 140981.

Deng L, Shangguan ZP, Li R. Effects of the grain-for-green program on soil erosion in China. International Journal of Sediment Research 2012; 27: 120-127.

Ding C, Huang W, Li Y, Zhao S, Huang F. Nonlinear Changes in Dryland Vegetation Greenness over East Inner Mongolia, China, in Recent Years from Satellite Time Series. Sensors (Basel) 2020; 20.

Ding YT, Zhang M, Qian XY, Li CR, Chen S, Wang WW. Using the geographical detector

technique to explore the impact of socioeconomic factors on PM2.5 concentrations in China. Journal of Cleaner Production 2019; 211: 1480-1490.

Farley KA, Jobbagy EG, Jackson RB. Effects of afforestation on water yield: a global synthesis with implications for policy. Global Change Biology 2005; 11: 1565-1576.

Feng X, Fu B, Piao S, Wang S, Ciais P, Zeng Z, et al. Revegetation in China's Loess Plateau is approaching sustainable water resource limits. Nature Climate Change 2016; 6: 1019-1022.

Fensholt R, Langanke T, Rasmussen K, Reenberg A, Prince SD, Tucker C, et al. Greenness in semi-arid areas across the globe 1981–2007 — an Earth Observing Satellite based analysis of trends and drivers. Remote Sensing of Environment 2012; 121: 144-158.

Fensholt R, Proud SR. Evaluation of Earth Observation based global long term vegetation trends — Comparing GIMMS and MODIS global NDVI time series. Remote Sensing of Environment 2012; 119: 131-147.

Forzieri G, Alkama R, Miralles DG, Cescatti A. Satellites reveal contrasting responses of regional climate to the widespread greening of Earth. Science 2017; 356: 1180-1184.

Howell TA, Dusek DA. Comparison of vapor pressure deficit calcullation methods southern high plains. Journal of irrigation and drainage engineering 1995; 121: 191-198.

Hu Z, Zhao W, Guo Q, Wu G, Chen R, Li S. Contributions of Climatic Factors to Interannual Variability of the Vegetation Index in Northern China Grasslands. Journal of Climate 2020; 33: 175-183.

Huang M, Piao S, Ciais P, Peñuelas J, Wang X, Keenan TF, et al. Air temperature optima of vegetation productivity across global biomes. Nat Ecol Evol 2019; 3: 772-779.

Keenan TF, Riley WJ. Greening of the land surface in the world's cold regions consistent with recent warming. Nat Clim Chang 2018; 8: 825-828.

Korth H, Tsyganenko NA, Johnson CL, Philpott LC, Anderson BJ, Al Asad MM, et al. Modular model for Mercury's magnetospheric magnetic field confined within the average observed magnetopause. J Geophys Res Space Phys 2015; 120: 4503-4518.

Li J, Peng S, Li Z. Detecting and attributing vegetation changes on China's Loess Plateau. Agricultural and Forest Meteorology 2017; 247: 260-270.

Li M-m, Liu A-t, Zou C-j, Xu W-d, Shimizu H, Wang K-y. An overview of the "Three-North" Shelterbelt project in China. Forestry Studies in China 2012; 14: 70-79.

Li Y, Piao S, Li LZX, Chen A, Wang X, Ciais P, et al. Divergent hydrological response to large-scale afforestation and vegetation greening in China. Sci Adv 2018; 4: eaar4182.

Liu D, Li Y, Wang T, Peylin P, MacBean N, Ciais P, et al. Contrasting responses of grassland water

and carbon exchanges to climate change between Tibetan Plateau and Inner Mongolia. Agricultural and Forest Meteorology 2018; 249: 163-175.

Luo L, Mei K, Qu L, Zhang C, Chen H, Wang S, et al. Assessment of the Geographical Detector Method for investigating heavy metal source apportionment in an urban watershed of Eastern China. Sci Total Environ 2019; 653: 714-722.

Nemani RR, Keeling CD, Hashimoto H, Jolly WM, Piper SC, Tucker CJ, et al. Climate-driven increases in global terrestrial net primary production from 1982 to 1999. Science 2003; 300: 1560-3.

Niu Q, Xiao X, Zhang Y, Qin Y, Dang X, Wang J, et al. Ecological engineering projects increased vegetation cover, production, and biomass in semiarid and subhumid Northern China. Land Degradation & Development 2019; 30: 1620-1631.

Peng SS, Chen AP, Xu L, Cao CX, Fang JY, Myneni RB, et al. Recent change of vegetation growth trend in China. Environmental Research Letters 2011; 6: 044027.

Peng SS, Piao SL, Shen ZH, Ciais P, Sun ZZ, Chen SP, et al. Precipitation amount, seasonality and frequency regulate carbon cycling of a semi-arid grassland ecosystem in Inner Mongolia, China: A modeling analysis. Agricultural and Forest Meteorology 2013; 178: 46-55.

Piao S, Yin G, Tan J, Cheng L, Huang M, Li Y, et al. Detection and attribution of vegetation greening trend in China over the last 30 years. Glob Chang Biol 2015; 21: 1601-9.

Piao SL, Fang JY, Zhou LM, Guo QH, Henderson M, Ji W, et al. Interannual variations of monthly and seasonal normalized difference vegetation index (NDVI) in China from 1982 to 1999. Journal of Geophysical Research-Atmospheres 2003; 108: 4401.

Piao SL, Mohammat A, Fang JY, Cai Q, Feng JM. NDVI-based increase in growth of temperate grasslands and its responses to climate changes in China. Global Environmental Change-Human and Policy Dimensions 2006; 16: 340-348.

Pinzon J, Tucker C. A Non-Stationary 1981–2012 AVHRR NDVI3g Time Series. Remote Sensing 2014; 6: 6929-6960.

Poulter B, Frank D, Ciais P, Myneni RB, Andela N, Bi J, et al. Contribution of semi-arid ecosystems to interannual variability of the global carbon cycle. Nature 2014; 509: 600-3.

Rawson HM, Begg JE, Woodward RG. The Effect of Atmospheric Humidity on Photosynthesis, Transpiration and Water Use Efficiency of Leaves of Several Plant Species. Planta 1977; 134: 5-10.

Ryo M, Aguilar-Trigueros CA, Pinek L, Muller LAH, Rillig MC. Basic Principles of Temporal Dynamics. Trends Ecol Evol 2019; 34: 723-733.

Schimel D, Melillo J, Tian H, McGuire AD, Kicklighter D, Kittel T, et al. Contribution of

increasing $CO_2$ and climate to carbon storage by ecosystems in the United States. Science 2000; 287: 2004-6.

Seddon AW, Macias-Fauria M, Long PR, Benz D, Willis KJ. Sensitivity of global terrestrial ecosystems to climate variability. Nature 2016; 531: 229-32.

Seymour F, Harris NL. Reducing tropical deforestation. Science 2019; 365: 756-757.

Strassburg BBN, Rodrigues ASL, Gusti M, Balmford A, Fritz S, Obersteiner M, et al. Impacts of incentives to reduce emissions from deforestation on global species extinctions. Nature Climate Change 2012; 2: 350-355.

Tian F, Fensholt R, Verbesselt J, Grogan K, Horion S, Wang YJ. Evaluating temporal consistency of long-term global NDVI datasets for trend analysis. Remote Sensing of Environment 2015; 163: 326-340.

Ukkola AM, Prentice IC, Keenan TF, van Dijk AIJM, Viney NR, Myneni Ranga B, et al. Reduced streamflow in water-stressed climates consistent with $CO_2$ effects on vegetation. Nature Climate Change 2015; 6: 75-78.

Wang F, Pan X, Gerlein- Safdi C, Cao X, Wang S, Gu L, et al. Vegetation restoration in Northern China: A contrasted picture. Land Degradation & Development 2020; 31: 669-676.

Wang JF, Li XH, Christakos G, Liao YL, Zhang T, Gu X, et al. Geographical Detectors- Based Health Risk Assessment and its Application in the Neural Tube Defects Study of the Heshun Region, China. International Journal of Geographical Information Science 2010; 24: 107-127.

Wang S, Fu B, Piao S, Lü Y, Ciais P, Feng X, et al. Reduced sediment transport in the Yellow River due to anthropogenic changes. Nature Geoscience 2015; 9: 38-41.

Wingate VR, Phinn SR, Kuhn N. Mapping precipitation-corrected NDVI trends across Namibia. Sci Total Environ 2019; 684: 96-112.

Wu Z, Wu J, He B, Liu J, Wang Q, Zhang H, et al. Drought offset ecological restoration program-induced increase in vegetation activity in the Beijing-Tianjin Sand Source Region, China. Environ Sci Technol 2014; 48: 12108-17.

Xu L, Myneni RB, Chapin FS, Callaghan TV, Pinzon JE, Tucker CJ, et al. Temperature and vegetation seasonality diminishment over northern lands. Nature Climate Change 2013; 3: 581-586.

Yu G, He H, Liu X. Atlas of Spatial Information in Chinese Terrestrial Ecosystems: Climate Volume. Meteorology Press, Beijing 2004; in Chinese.

Yu LX, Liu Y, Liu TX, Yan FQ. Impact of recent vegetation greening on temperature and precipitation over China. Agricultural and Forest Meteorology 2020; 295.

Yuan W, Zheng Y, Piao S, Ciais P, Lombardozzi D, Wang Y, et al. Increased atmospheric vapor pressure deficit reduces global vegetation growth. Sci Adv 2019; 5: eaax1396.

Zhang B, He C, Burnham M, Zhang L. Evaluating the coupling effects of climate aridity and vegetation restoration on soil erosion over the Loess Plateau in China. Sci Total Environ 2016a; 539: 436-449.

Zhang T, Peng J, Liang W, Yang Y, Liu Y. Spatial-temporal patterns of water use efficiency and climate controls in China's Loess Plateau during 2000-2010. Sci Total Environ 2016b; 565: 105-122.

Zhang Y, Peng C, Li W, Tian L, Zhu Q, Chen H, et al. Multiple afforestation programs accelerate the greenness in the 'Three North' region of China from 1982 to 2013. Ecological Indicators 2016c; 61: 404-412.

Zhao W, Hu Z, Li S, Guo Q, Liu Z, Zhang L. Comparison of surface energy budgets and feedbacks to microclimate among different land use types in an agro-pastoral ecotone of northern China. Sci Total Environ 2017; 599-600: 891-898.

Zhao Y, Deng Q, Lin Q, Zeng C, Zhong C. Cadmium source identification in soils and high-risk regions predicted by geographical detector method. Environ Pollut 2020; 263: 114338.

Zheng H, Lin H, Zhou W, Bao H, Zhu X, Jin Z, et al. Revegetation has increased ecosystem water-use efficiency during 2000–2014 in the Chinese Loess Plateau: Evidence from satellite data. Ecological Indicators 2019; 102: 507-518.

Zhou LM, Tucker CJ, Kaufmann RK, Slayback D, Shabanov NV, Myneni RB. Variations in northern vegetation activity inferred from satellite data of vegetation index during 1981 to 1999. Journal of Geophysical Research-Atmospheres 2001; 106: 20069-20083.

Zhou S, Williams AP, Berg AM, Cook BI, Zhang Y, Hagemann S, et al. Land-atmosphere feedbacks exacerbate concurrent soil drought and atmospheric aridity. Proc Natl Acad Sci U S A 2019; 116: 18848-18853.

Zhu ZC, Piao SL, Myneni RB, Huang MT, Zeng ZZ, Canadell JG, et al. Greening of the Earth and its drivers. Nature Climate Change 2016; 6: 1-6.

# Credit author statement

**Zhao Wei:** Conceptualization, Methodology, Data curation, Writing- Original draft preparation **Yu Xiubo**: Conceptualization, Writing- Reviewing **Jiao Cuicui**: Conceptualization, Investigation **Xu Chengdong**: Software, Writing- Reviewing **Liu Yu**: Writing - Original Draft, Validation. **Wu Genan:** Data curation and Editing.

## Declaration of competing interest

The authors declare that they have no known competing financial interests or personal relationships that could have appeared to influence the work reported in this paper.

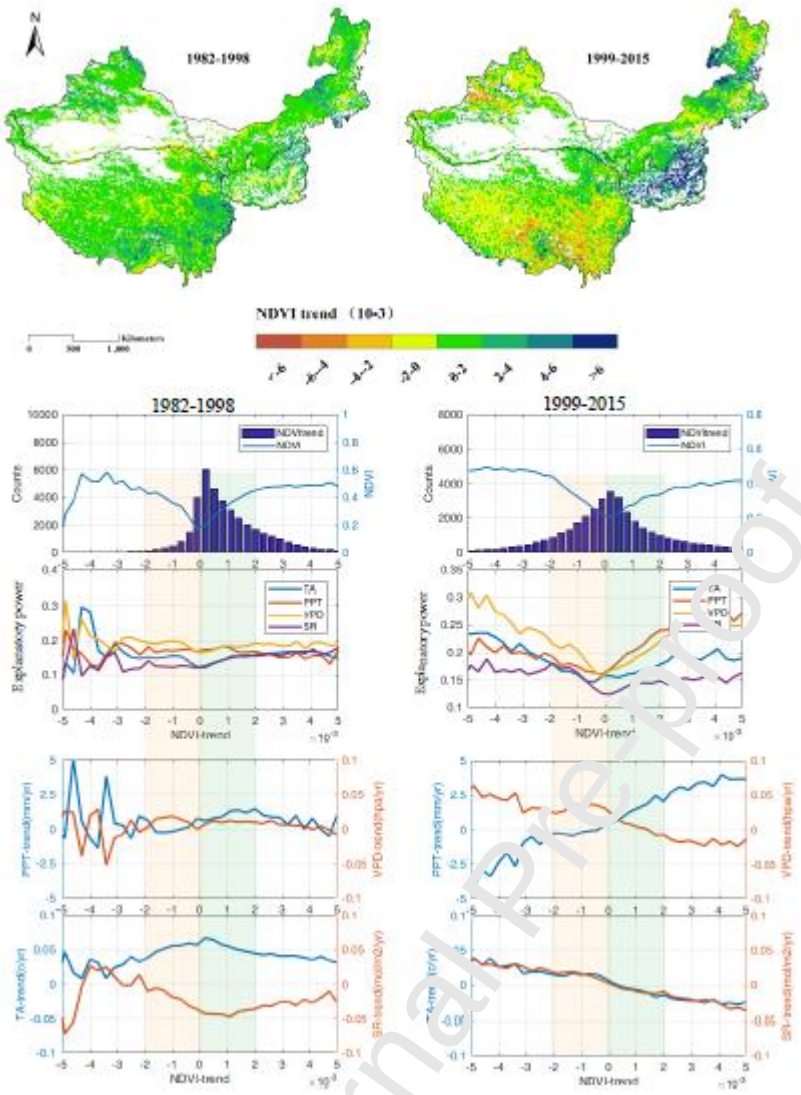


Graphical abstract

**Highlights**

- NDVI trends with weaker greening but greater spatial heterogeneity after1999.
- Loess Plateau had high greening but Tibet Plateau showed mean browning post-1999.
- Association in variability of climate and vegetation were strengthened after 1999.
- PPT and VPD are most closely related to the IAV of NDVI in 1982-1998 and 1999-2015.
- NDVI trends were corresponding to changes in PPT and VPD post-1999 but no pre-1999.